Holey Graphene as a Weed Barrier for Molecules

Matthew L. Gethers,[†,‡] John C. Thomas,[§] Shan Jiang,[§] Nathan O. Weiss,[⊥] Xiangfang Duan,[*,§] William A. Goddard, III,[*,†,∥,#] and Paul S. Weiss[*,§,⊥]

[†]Materials and Process Simulation Center and [‡]Department of Biological Engineering, California Institute of Technology, Pasadena, California 91125, United States, [§]Department of Chemistry and Biochemistry and California NanoSystems Institute and [⊥]Department of Materials Science and Engineering, University of California, Los Angeles, Los Angeles, California 90095, United States, and [∥]Department of Chemistry, and [#]Department of Materials Science, Chemistry, California Institute of Technology, Pasadena, California 91125, United States

ABSTRACT We demonstrate the use of "holey" graphene as a mask against molecular adsorption. Prepared porous graphene is transferred onto a Au{111} substrate, annealed, and then exposed to dilute solutions of 1-adamantanethiol. In the pores of the graphene lattice, we find islands of organized, self-assembled molecules. The bare Au in the pores can be regenerated by postdeposition annealing, and new molecules can be self-assembled in the exposed Au region. Graphene can serve as a robust, patternable mask against the deposition of self-assembled monolayers.

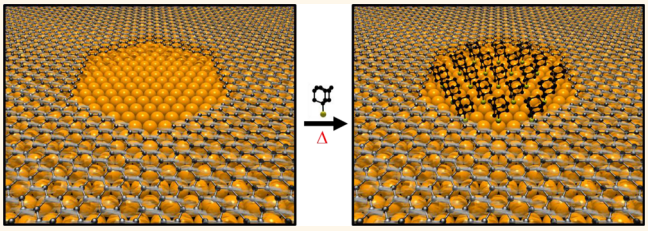

KEYWORDS: nanoscience · graphene · mask · chemical patterning · self-assembly · scanning tunneling microscopy

The extraordinary electronic, thermal, and mechanical properties of graphene have been elaborated and exploited.[1] Graphene's high carrier mobility and ambipolarity make it a potentially powerful component in electronic systems.[2] An equally intriguing aspect of graphene is its capacity to act as an impermeable or semipermeable membrane; Bunch *et al.* demonstrated the impermeability of graphene to helium through the inflation of a "nanoballoon".[3,4] Graphene can also act as an effective barrier to oxidation of metal surfaces under certain conditions.[5−7] The purposeful introduction of pores into graphene tunes this permeability by allowing certain molecules to pass through while others are inhibited. This use of graphene has led to proposals as varied as desalination and DNA sequencing.[8−14] Here, we demonstrate and explore the use of "holey" graphene as a molecular barrier by applying it to adsorption and self-assembly.

Self-assembly provides a convenient route toward the bottom-up placement of single molecules with applications ranging from nanotechnology to biology.[15−18] Molecules for self-assembly typically comprise an attaching head group, an interacting backbone, and a functional tail group. The head group binds the molecule to a substrate; backbone intermolecular interactions lead to crystalline packing (through design), and the exposed terminal functional group can tune interfacial chemical properties between the substrate and its environment.[19] Molecular monolayers enable controllable surface functionalization and can be used to isolate and to study individual molecules.[20−22] Self-assembly is made even more powerful when combined with patterning. Currently, patterning of self-assembled monolayers (SAMs) is achieved through conventional, soft, or hybrid lithographies that are limited by the conflicting requirements of feature resolution and large-scale fabrication, where manufacturing cost and assembly time play key roles.[23−27] Inspired by the approach of Battaglini *et al.*, we pattern SAMs by masking the surface with an inert material.[28] We find that graphene can function as such a mask, as it is a material with relatively inert chemistry[29] and functions as an impermeable barrier against other molecules. Our choice was also influenced by the number of techniques that enable the introduction of nanoscale pores of arbitrary size and location to graphene, including both electron-beam bombardment and chemical approaches.[30−39] These techniques will ultimately provide

* Address correspondence to psw@cnsi.ucla.edu, wag@wag.caltech.edu, xduan@chem.ucla.edu.

Received for review June 27, 2015 and accepted October 1, 2015.

Published online October 01, 2015
10.1021/acsnano.5b03936

flexibility and precision in pattern shape and scale, including precise hole size and pitch. Used in this way, graphene acts as a "weed barrier", where it restricts covered areas from forming Au−S attachments (molecules "taking root") and thus enables only the open regions exposed by the pores to form substrates covered by self-assembled monolayers (akin to gardening where, ideally, plants only grow in the holes deliberately placed in the weed barrier).

At the same time, the graphene−Au interaction is relatively weak, as observed in a number of quantitative and spectroscopic studies of aromatics on Au{111}.[40−43] For example, aromatics sit much farther from and interact much less strongly with the Au{111} surface than from the close-packed Ag{111} and Cu{111} surfaces.[43]

RESULTS AND DISCUSSION

The process we developed for producing spatially patterned monolayers on Au{111} using a graphene mesh is shown schematically in Figure 1. We fabricate "holey" graphene by depositing graphene on a SiO_2 substrate[44−46] and then evaporate a thin layer of Au (2 nm) onto the exposed graphene layer. Subsequent annealing forms surface-bound Au nanoparticles. The Au nanoparticles catalyze oxidation of the graphene by oxygen in the air, thereby forming pores. The Au nanoparticles are then etched *via* brief immersion into an etchant solution (see Materials and Methods for details). A thin protecting layer of poly(methyl methacrylate) (PMMA) is added to facilitate transfer, and the "holey" graphene is transferred onto a Au{111} substrate. The protecting layer is removed, and samples are ready for characterization. Further annealing at 100 °C removes any excess solvent, and the covered Au{111} substrate is thereby primed for molecular deposition. We confirm the fabrication of porous graphene by transmission electron microscopy (TEM), where TEM images show a graphene mesh with randomly distributed holes; measured holes have an average diameter of 37 ± 8 Å (Figure 2 and Figure S1). Images also depict cracks in the graphene induced by

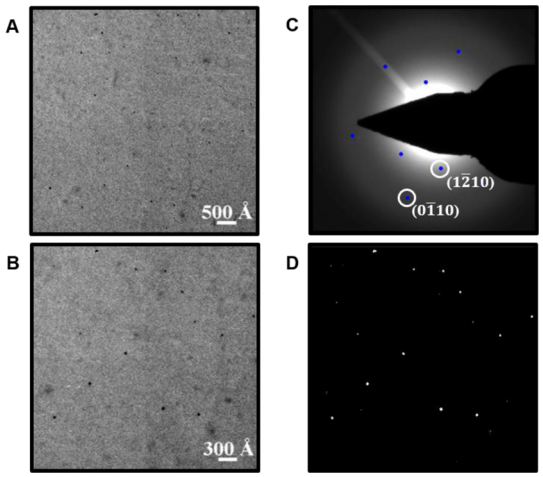

Figure 2. (A,B) "Holey" graphene measured with transmission electron microscopy supported on a 200 mesh Formvar/copper grid. Each image was acquired at an accelerating voltage of 300 kV using a FEI Titan microscope. Holes measured with TEM are 37 ± 8 Å in diameter and are randomly distributed across the graphene layer. (C) Diffraction image of B is shown, where the hexagonal pattern of graphene is observed. Orientation points are highlighted, for clarity, in blue, where local image maxima were computed within a defined pixel window. (D) Thresholded binary of B that highlights randomly distributed holes within the graphene mesh.

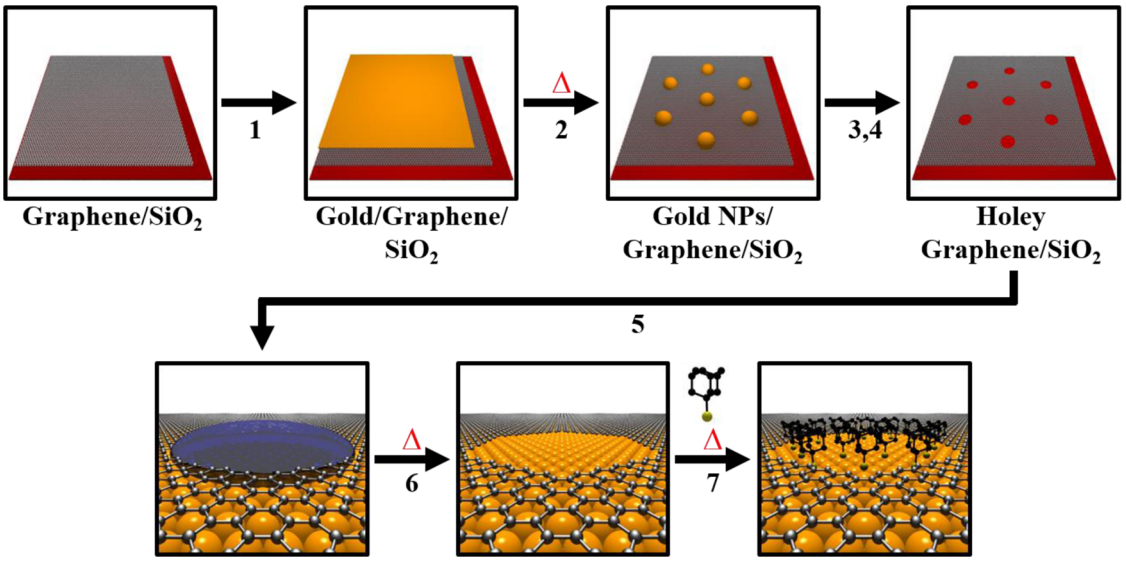

Figure 1. Process for producing spatially patterned monolayers on Au{111} using a graphene mesh. From a monolayer sheet of graphene on a SiO_2 substrate, (1) 2 nm of Au is deposited and (2) then annealed for 15 min at 350 °C. (3) The Au is etched (KI/I_2, solution) for 30 s and (4) washed in DI water for 30 s. (5) "Holey" graphene is then transferred to a Au{111}/mica substrate and (6) annealed at 100 °C for 24 h. (7) The same substrate is then exposed to the vapor of a 1 mM ethanolic solution of 1-adamantanethiol (1AD) at 78 °C for 24 h for deposition.

the transfer and annealing processes. Graphene is known to retain the surface morphology of the substrate on which it was synthesized even when attached to the PMMA overlayer.[47] When transferred to the final substrate, this morphology results in gaps between the graphene and the substrate that can cause folding and cracking when the PMMA is removed. Further, water caught between the graphene and the substrate can leave gaps between the graphene and substrate upon drying that lead to folds, thereby appearing like graphite in images.[47] After the mesh is successfully transferred to Au{111} and annealed, we use scanning tunneling microscopy (STM) to probe the local environment.

The scanning tunneling microscope provides a window into the nanoscopic world, where constant-current imaging measures a convolution of electronic and topographic structure as a function of position across surfaces.[48−50] Measurements are recorded on a custom-built, ultrastable microscope held at ambient temperature and pressure.[51] Scanning tunneling micrographs before annealing are shown in Figure S2, where we note a large depression (pore) in the center of the image that is surrounded by other pores filled with residual solvent from the transfer step. Annealing removes the solvent within the pores. The annealed graphene−gold surface is shown in Figure 3, where images depict porous graphene with hole diameters that match those in TEM measurements. The surrounding graphene Moiré pattern shows a six-fold symmetry with a nearest-neighbor distance of 5.0 ± 0.5 Å, which is in good agreement with the predicted and energetically favorable (2 × 2) superstructure for graphene on a Au{111} substrate.[52]

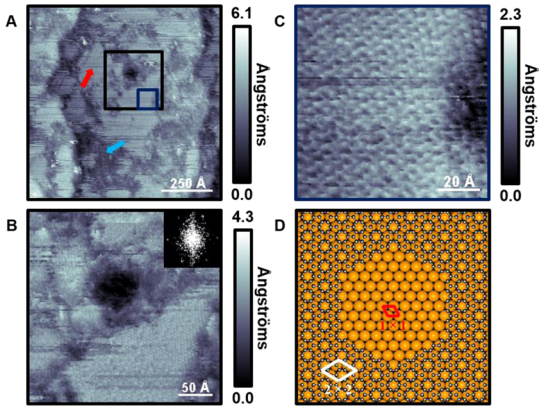

Figure 3. (A) Scanning tunneling micrograph ($I_{tunneling}$ = 3 pA, V_{sample} = −1.0 V) of "holey" graphene on Au{111}/mica along two monatomic step edges after annealing at 100 °C for 24 h. We highlight an ordered region (red arrow, higher in conductance) and an area of disorder (blue arrow, lower in conductance) that we attribute to possible cracks, folds, and varied underlying graphene−Au attachments. (B) Higher resolution of the larger box in A. (C) Higher resolution image of the smaller box in A. Inset in B shows a fast Fourier transform, where graphene displays hexagonal nearest-neighbor spacings of 5.0 ± 0.5 Å. (D) Schematic showing a pore in graphene exposing the underlying Au{111} substrate that further depicts the measured (2 × 2) Moiré superstructure of graphene on Au.

The structure of graphene on Au{111} is difficult to predict and likely to be locally varied, where measured superlattices are highly influenced by both the underlying Au substrate and the detailed structure of the STM tip.[44,53] With this caveat in mind, acquired STM images confirm a single transferred layer of holey graphene with exposed Au regions, where image differences were quantified in real and Fourier space. Thresholding and masking techniques, performed in MATLAB, enable gold and graphene regions to be segmented and compared (Figure S3). In STM images, under the conditions used, graphene layers are 2.1 ± 1.1 Å more protruding in apparent height compared to exposed Au regions. The same sample is then exposed to the vapor of a 1 mM ethanolic solution of the self-assembling cage molecule 1-adamantanethiol (**1AD**) and subsequently imaged.[54]

The diamondoid **1AD** is ideal for an initial patterning test, in that it is commercially available, forms well-ordered monolayers with few defects (due to limited degrees of freedom), and has a well-defined structure.[55−58] Scanning tunneling micrographs recorded after deposition show islands of molecular protrusions consistent with the diameters of the pores (Figure 4). Nearest-neighbor distances within measured molecular protrusions (7.2 ± 1.1 Å) are near previously recorded distances of **1AD** on Au{111} (6.9 ± 0.4 Å) (Figure S4).[55,59] The areas surrounding the islands proved difficult to resolve; however, there were small, well-resolved areas bearing molecular features that were analyzed (Figure S5). Several of these areas topographically resemble the graphene overlayer imaged prior to **1AD** deposition. The average nearest-neighbor spacing of these areas (5.0 ± 1.1 Å) is

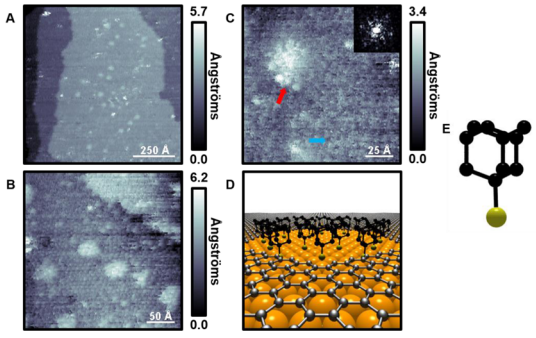

Figure 4. (A) Scanning tunneling micrograph ($I_{tunneling}$ = 3 pA, V_{sample} = −1.0 V) of "holey" graphene on Au{111}/mica after exposure to the vapor of a 1 mM ethanolic solution of 1AD. (B,C) Two regions where 1AD has assembled on Au{111} within the confines of the pores of the holey graphene. Here, we highlight protrusions due to 1AD (red arrow) and areas of graphene (blue arrow) for clarity. (C, inset) Fast Fourier transform shows local order of the graphene overlayer with nearest-neighbor spacings of 5.0 ± 1.1 Å. Molecular distances for 1AD were computed in real space, with nearest-neighbor spacings of 7.2 ± 1.1 Å (see Figure S4 for more detail). (D) Schematic of the arrangement in C, where the graphene pore is filled with assembled 1AD. (E) Ball-and-stick model of the 1AD molecule with hydrogens not shown.

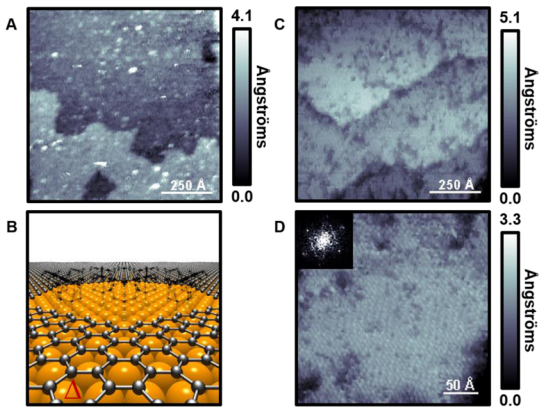

Figure 5. (A) Scanning tunneling micrograph ($I_{tunneling}$ = 3 pA, V_{sample} = −1.0 V) of "holey" graphene with the 2D pores filled with assembled 1-adamantanethiol on Au{111}/mica. (B) Annealing at 250 °C for 24 h removes adsorbates from the pores, as shown schematically. (C,D) Scanning tunneling micrographs ($I_{tunneling}$ = 3 pA, V_{sample} = −1.0 V) of the same sample after complete molecular desorption, recorded at two different resolutions, as indicated. (D, inset) Fast Fourier transform shows the recovered hexagonal spacing (5.0 ± 0.5 Å) measured previously.

consistent with the graphene overlayer. The difference in nearest-neighbor spacings provides evidence of separate molecular domains brought about due to the graphene-masking effect against the deposition of **1AD**. Graphene regions show a different apparent height than **1AD** islands and can thereby be segmented (Figure S6), where **1AD** patches differ by 1.1 ± 0.5 Å in the *z*-direction under the STM imaging conditions used. Measured spacings, both in the lateral and surface-normal (apparent height) directions, and consistent hole diameters confirm the blocking effect of the graphene layer. The same samples are then annealed again to test if molecular desorption can be achieved and thus if the bare surface in the pores of the graphene mask can be regenerated.

Scanning tunneling topographs before and after this second anneal, to 250 °C, are shown in Figure 5, where evidence of molecular desorption is obtained.[18,60,61] Once-filled holes are now empty, and the hexagonal spacing of 5.0 ± 0.5 Å is recovered outside graphene pores. We confirm desorption by topographic imaging, where the exposed areas within the mask are destructively regenerated and thus prepared for further molecular deposition steps (Figure S7). We suggest that nondestructive methods such as displacement techniques could also be applied since **1AD** has been shown to be labile upon exposure *via* solution, vapor, or contact to more strongly bound self-assembling molecules.[57,58]

CONCLUSIONS AND PROSPECTS

The effectiveness of graphene as a mask against adsorption depends on the integrity of the graphene. Defects, folds, wrinkles, and strain can all compromise the impermeability of the mask. Small defects and cracking permit penetration of adsorbates through to the underlying substrate. Folding leads to multilayered regions where a pore in one layer can be occluded by another layer that is not porous. A strained lattice could open gaps in the mesh and induce tearing at pores. Second to the synthesis of the graphene itself, the transfer of the graphene to the target substrate is the most important process in minimizing these undesirable features. Improving the transfer method can alleviate some of these issues. Liang *et al.* point out several ways in which the transfer can be improved, including increasing the hydrophobicity of the target substrate, annealing the graphene/substrate complex before dissolving the PMMA, and using the modified "RCA Clean" method to get rid of residual agents.[47,62−65] While our method patterns graphene destructively, another approach is to employ bottom-up methods to graphene synthesis that enable the placement and design of desired structures with predetermined pore size, shape, and pitch.[66−69]

The graphene mask approach embodies a wholly different set of strengths and weaknesses than photolithographic and soft-lithography approaches.[24,26] Patterning is achieved with electron-beam and chemical methods, surpassing the diffraction limit of photolithographic methods and placing it in league with scanning probe lithography in feature size. The graphene mask, akin to the PDMS stamp and unlike the scanning probe lithography techniques, is reusable and can cover large areas. Our approach permits control over the pattern, overcoming a major limitation of Battaglini's approach, though it is not removable and thus cannot be backfilled. The value of graphene as a mask is further enhanced by its thermal stability, making it resilient to high-temperature fabrication processes.[70] Importantly for SAMs, thermal stability implies that the integrity of the graphene should not be compromised when annealing the masked substrate to remove adsorbates and thereby to regenerate the mask.

Our results show that graphene can serve as a barrier to adsorption and open up a plethora of future patterning experiments. Since graphene pores can be readily manufactured, masks can be used with a wide variety adsorbates with implications ranging from constructing well-defined nanoarchitectures to patterning biosensors.

MATERIALS AND METHODS

Holey Graphene Sample Preparation. Graphene was synthesized on a 25 mm thick copper foil (99.8%, Alfa Aesar, Ward Hill, MA) that was treated with hydrochloric acid/deionized water (1:10) (36.5−38.0%, Sigma-Aldrich, St. Louis, MO) for 30 min and rinsed by isopropyl alcohol (99.8%, Sigma-Aldrich, St. Louis, MO) for 10 min. After being dried under a N_2 stream, the copper foil was loaded into the chemical vapor deposition (CVD) furnace (1 in. tube diameter; Lindbergh/Blue M, Thermo Scientific, Waltham, MA). The system was pumped down to a vacuum

of 10 mTorr in 30 min and refilled with 300 sccm H_2/Ar flow (25 sccm/475 sccm) and heated to 1040 °C within 25 min. Next, diluted methane and Ar were introduced into the CVD system for graphene growth at 1040 °C for 90 min (500 ppm methane in Ar, 35 sccm) with H_2/Ar (25 sccm/440 sccm). All process gases were supplied by Airgas, Inc. (Burbank, CA).

Graphene was grown on both sides of the copper foil, and one side of the graphene/copper surface was spin-coated with poly(methyl methacrylate) (495 PMMA C_2, MicroChem, Newton, MA) and baked at 140 °C for 5 min. The other side of the copper foil was exposed to O_2 plasma for 1 min to remove the graphene. After that, the Cu foil was etched away using copper etchant (ferric chloride, Transene), resulting in a free-standing PMMA/graphene membrane floating on the surface of the etchant bath. The PMMA/graphene film was washed with HCl/deionized H_2O (1:10) and deionized water several times and then transferred onto a 300 nm thick SiO_2 substrate. After being air-dried, the PMMA was dissolved by acetone and the substrate was rinsed with isopropyl alcohol to yield a graphene film on the substrate.

A 2-nm-thick gold film was deposited using thermal evaporation onto the graphene/SiO_2 substrate. After being annealed at 350 °C for 15 min, gold nanoparticles were found on the substrate. The holey graphene was oxidized by exposure to oxygen in the ambient air, with gold nanoparticles acting as the catalyst. The gold nanoparticles were removed by gold etchant (KI/I_2 solution, Sigma-Aldrich, St. Louis, MO) and washed with isopropyl alcohol and deionized water. The graphene/SiO_2 was again spin-coated with PMMA, and the SiO_2 substrate was etched away using a buffered oxide etch. The PMMA-coated holey graphene was washed in deionized water and transferred to a deionized water bath. A H_2 flame-annealed (at a rate of 1 Hz, 10 passes) Au{111}/mica substrate (Agilent, Santa Clara, CA) was then used to scoop the PMMA-coated graphene from the water bath. The PMMA/graphene/Au substrate was allowed to air-dry overnight, and then the PMMA was dissolved in acetone and the graphene/Au substrate was washed with isopropyl alcohol.

Transmission Electron Microscopy. The morphology and structure of the graphene were characterized with field emission high-resolution transmission electron microscopy (FEI Titan S/TEM), typically at an accelerating voltage of 300 kV. The diffraction patterns were collected with accelerating voltages of 300 kV to assess whether the beam energy played a role in graphene surface changes. Specimens for TEM analysis were prepared by the same process as that for graphene transfer onto 200 mesh Formvar/copper grids purchased from Ted Pella, Inc. (Redding, CA).

Scanning Tunneling Microscope Sample Preparation. Holey graphene was deposited onto flame-annealed, commercially available Au{111} on mica substrates. Samples were imaged and then subsequently annealed at 100 °C for a period of 24 h in a gasketed glass v-vial (Wheaton, Millville, NJ). Samples were heated in a chamber of a Barstead Thermolyne 1400 furnace (ThermoFischer Scientific, Waltham, MA). Samples were taken out and imaged with STM and then placed back into a clean v-vial above a solution of 1 mM commercially available 1-adamantanethiol (Sigma-Aldrich, St. Louis, MO) in ethanol for vapor deposition. Vials were placed back into a preheated furnace at 78 °C for a period of 24 h. Inserted 1-adamantanethiolate holey graphene samples were taken out for STM imaging. After sufficient experiments were performed, samples were placed back into a preheated furnace at 250 °C for a period of 24 h for molecular desorption. Samples were then taken out for subsequent imaging and desorption confirmation.

Imaging. All STM measurements were performed in air using a custom beetle-style scanning tunneling microscope and a platinum/iridium tip (80:20).[51] The known lattice of 1-dodecanethiolate SAMs on Au{111} was used to calibrate the piezoelectric scanners. The sample was held between −1 V and −0.1 V bias range, and 256 × 256 pixel images were collected, at varying size, in constant-current mode with a tunneling current ranging from 2 to 80 pA. There is a strong tip dependence for imaging cage molecules, as reported previously.[71]

Image Analyses. All STM images were initially processed with automated routines developed in MATLAB (Mathworks, Natick, MA) to remove any high-frequency noise and intensity spikes that may otherwise impair reliable segmentation.[49] Images used to obtain nearest-neighbor spacings were resized to account for drift at room temperature. Transmission electron microscopy images were thresholded to segment both graphene holes and the graphene layer that was used to create a binary mask, where the average diameter of the holes was computed. Orientations in diffraction images obtained by TEM were highlighted by computing local maxima within a defined pixel radius (10 pixels), referenced, and plotted for clarity. The nearest-neighbor spacing of graphene was computed in Fourier space for the pre-1-adamantanethiol deposition and post-annealing experiments. The spacings of assembled 1-adamantanethiol and the surrounding graphene were determined by fitting the centers of the molecules using a binary mask generated through thresholding and the Regionprops function in Matlab. Values obtained by Fourier analysis and Regionprops fitting on the same image were compared to ensure that results were similar. Apparent height was also used for image segmentation and to determine separation distances in the *z*-direction.

Conflict of Interest: The authors declare no competing financial interest.

Supporting Information Available: The Supporting Information is available free of charge on the ACS Publications website at DOI: 10.1021/acsnano.5b03936.

Transmission electron microscope images that show hole diameter analysis, freshly deposited "holey" graphene on Au{111} before and after heating, STM images used to compute nearest neighbor spacings, and thresholding analyses used to segment molecular layers (PDF)

Acknowledgment. We thank the Department of Energy Grant #DE-SC-0005025 for support of the instrumentation and methods developed and applied here. Partial support was provided by NSF Grant #ODISSEI-EFRI-1332411 and the Caltech EAS Discovery Fund (M.G. and W.A.G.). We also thank the NSF (Grant #EFRI-1433541) for support (X.F.D., S.J., and N.O.W.). J.C.T. acknowledges support from an excellence in chemistry graduate research fellowship from UCLA. P.S.W. acknowledges support from the Caltech Kavli Nanoscience Institute and Joint Center for Artificial Photosynthesis. We gratefully thank Jeffrey J. Schwartz, Ivo Atanasov, and Chih-Yen Chen for helpful discussions.

REFERENCES AND NOTES

1. Novoselov, K. S.; Geim, A. K.; Morozov, S. V.; Jiang, D.; Zhang, Y.; Dubonos, S. V.; Grigorieva, I. V.; Firsov, A. A. Electric Field Effect in Atomically Thin Carbon Films. *Science* **2004**, *306*, 666–669.
2. Allen, M. J.; Tung, V. C.; Kaner, R. B. Honeycomb Carbon: A Review of Graphene. *Chem. Rev.* **2010**, *110*, 132–145.
3. Bunch, J. S.; Verbridge, S. S.; Alden, J. S.; van der Zande, A. M.; Parpia, J. M.; Craighead, H. G.; McEuen, P. L. Impermeable Atomic Membranes from Graphene Sheets. *Nano Lett.* **2008**, *8*, 2458–2462.
4. Berry, V. Impermeability of Graphene and Its Applications. *Carbon* **2013**, *62*, 1–10.
5. Prasai, D.; Tuberquia, J. C.; Harl, R. R.; Jennings, G. K.; Bolotin, K. I. Graphene: Corrosion-Inhibiting Coating. *ACS Nano* **2012**, *6*, 1102–1108.
6. Nilsson, L.; Andersen, M.; Balog, R.; Lægsgaard, E.; Hofmann, P.; Besenbacher, F.; Hammer, B.; Stensgaard, I.; Hornekær, L. Graphene Coatings: Probing the Limits of the One Atom Thick Protection Layer. *ACS Nano* **2012**, *6*, 10258–10266.
7. Schriver, M.; Regan, W.; Gannett, W. J.; Zaniewski, A. M.; Crommie, M. F.; Zettl, A. Graphene as a Long-Term Metal Oxidation Barrier: Worse Than Nothing. *ACS Nano* **2013**, *7*, 5763–5768.
8. Sint, K.; Wang, B.; Král, P. Selective Ion Passage through Functionalized Graphene Nanopores. *J. Am. Chem. Soc.* **2008**, *130*, 16448–16449.

9. Schneider, G. F.; Kowalczyk, S. W.; Calado, V. E.; Pandraud, G.; Zandbergen, H. W.; Vandersypen, L. M. K.; Dekker, C. DNA Translocation through Graphene Nanopores. *Nano Lett.* **2010**, *10*, 3163–3167.
10. Merchant, C. A.; Healy, K.; Wanunu, M.; Ray, V.; Peterman, N.; Bartel, J.; Fischbein, M. D.; Venta, K.; Luo, Z.; Johnson, A. T. C. DNA Translocation through Graphene Nanopores. *Nano Lett.* **2010**, *10*, 2915–2921.
11. Garaj, S.; Hubbard, W.; Reina, A.; Kong, J.; Branton, D.; Golovchenko, J. A. Graphene as a Subnanometre Trans-Electrode Membrane. *Nature* **2010**, *467*, 190–193.
12. Siwy, Z. S.; Davenport, M. Nanopores: Graphene Opens up to DNA. *Nat. Nanotechnol.* **2010**, *5*, 697–698.
13. Cohen-Tanugi, D.; Grossman, J. C. Water Desalination Across Nanoporous Graphene. *Nano Lett.* **2012**, *12*, 3602–3608.
14. Russo, P.; Hu, A.; Compagnini, G. Synthesis, Properties and Potential Applications of Porous Graphene: A Review. *Nano-Micro Lett.* **2013**, *5*, 260–273.
15. Ulman, A. Formation and Structure of Self-Assembled Monolayers. *Chem. Rev.* **1996**, *96*, 1533–1554.
16. Poirier, G. E. Characterization of Organosulfur Molecular Monolayers on Au (111) Using Scanning Tunneling Microscopy. *Chem. Rev.* **1997**, *97*, 1117–1128.
17. Smith, R. K.; Lewis, P. A.; Weiss, P. S. Patterning Self-Assembled Monolayers. *Prog. Surf. Sci.* **2004**, *75*, 1–68.
18. Love, J. C.; Estroff, L. A.; Kriebel, J. K.; Nuzzo, R. G.; Whitesides, G. M. Self-Assembled Monolayers of Thiolates on Metals as a Form of Nanotechnology. *Chem. Rev.* **2005**, *105*, 1103–1170.
19. Claridge, S. A.; Liao, W.-S.; Thomas, J. C.; Zhao, Y.; Cao, H. H.; Cheunkar, S.; Serino, A. C.; Andrews, A. M.; Weiss, P. S. From the Bottom Up: Dimensional Control and Characterization in Molecular Monolayers. *Chem. Soc. Rev.* **2013**, *42*, 2725–2745.
20. Donhauser, Z. J.; Mantooth, B. A.; Kelly, K. F.; Bumm, L. A.; Monnell, J. D.; Stapleton, J. J.; Price, D. W.; Rawlett, A. M.; Allara, D. L.; Tour, J. M.; *et al.* Conductance Switching in Single Molecules through Conformational Changes. *Science* **2001**, *292*, 2303–2307.
21. Shuster, M. J.; Vaish, A.; Szapacs, M. E.; Anderson, M. E.; Weiss, P. S.; Andrews, A. M. Biospecific Recognition of Tethered Small Molecules Diluted in Self-Assembled Monolayers. *Adv. Mater.* **2008**, *20*, 164–167.
22. Weiss, P. S. Functional Molecules and Assemblies in Controlled Environments: Formation and Measurements. *Acc. Chem. Res.* **2008**, *41*, 1772–1781.
23. Gates, B. D.; Xu, Q.; Stewart, M.; Ryan, D.; Willson, C. G.; Whitesides, G. M. New Approaches to Nanofabrication: Molding, Printing, and Other Techniques. *Chem. Rev.* **2005**, *105*, 1171–1196.
24. Srinivasan, C.; Mullen, T. J.; Hohman, J. N.; Anderson, M. E.; Dameron, A. A.; Andrews, A. M.; Dickey, E. C.; Horn, M. W.; Weiss, P. S. Scanning Electron Microscopy of Nanoscale Chemical Patterns. *ACS Nano* **2007**, *1*, 191–201.
25. Willson, C. G.; Roman, B. J. The Future of Lithography: SEMATECH Litho Forum 2008. *ACS Nano* **2008**, *2*, 1323–1328.
26. Saavedra, H. M.; Mullen, T. J.; Zhang, P.; Dewey, D. C.; Claridge, S. A.; Weiss, P. S. Hybrid Strategies in Nanolithography. *Rep. Prog. Phys.* **2010**, *73*, 036501.
27. Liao, W.-S.; Cheunkar, S.; Cao, H. H.; Bednar, H. R.; Weiss, P. S.; Andrews, A. M. Subtractive Patterning via Chemical Lift-Off Lithography. *Science* **2012**, *337*, 1517–1521.
28. Battaglini, N.; Qin, Z.; Campiglio, P.; Repain, V.; Chacon, C.; Rousset, S.; Lang, P. Directed Growth of Mixed Self-Assembled Monolayers on a Nanostructured Template: A Step Toward the Patterning of Functional Molecular Domains. *Langmuir* **2012**, *28*, 15095–15105.
29. Yan, L.; Zheng, Y. B.; Zhao, F.; Li, S.; Gao, X.; Xu, B.; Weiss, P. S.; Zhao, Y. Chemistry and Physics of a Single Atomic Layer: Strategies and Challenges for Functionalization of Graphene and Graphene-Based Materials. *Chem. Soc. Rev.* **2012**, *41*, 97–114.
30. Fischbein, M. D.; Drndić, M. Electron Beam Nanosculpting of Suspended Graphene Sheets. *Appl. Phys. Lett.* **2008**, *93*, 113107.
31. Jin, Z.; Sun, W.; Yin, P.; Strano, M. S. Nanolithography Based on Metalized DNA Templates for Graphene Patterning. *Current Protocols in Chemical Biology*; John Wiley & Sons, Inc.: Hoboken, NJ, 2009; Vol. 6, pp 53–64.
32. Bai, J.; Zhong, X.; Jiang, S.; Huang, Y.; Duan, X. Graphene Nanomesh. *Nat. Nanotechnol.* **2010**, *5*, 190–194.
33. Song, B.; Schneider, G. F.; Xu, Q.; Pandraud, G.; Dekker, C.; Zandbergen, H. Atomic-Scale Electron-Beam Sculpting of Near-Defect-Free Graphene Nanostructures. *Nano Lett.* **2011**, *11*, 2247–2250.
34. Liu, J.; Cai, H.; Yu, X.; Zhang, K.; Li, X.; Li, J.; Pan, N.; Shi, Q.; Luo, Y.; Wang, X. Fabrication of Graphene Nanomesh and Improved Chemical Enhancement for Raman Spectroscopy. *J. Phys. Chem. C* **2012**, *116*, 15741–15746.
35. Radich, J. G.; Kamat, P. V. Making Graphene Holey. Gold-Nanoparticle-Mediated Hydroxyl Radical Attack on Reduced Graphene Oxide. *ACS Nano* **2013**, *7*, 5546–5557.
36. Xu, Q.; Wu, M.-Y.; Schneider, G. F.; Houben, L.; Malladi, S. K.; Dekker, C.; Yucelen, E.; Dunin-Borkowski, R. E.; Zandbergen, H. W. Controllable Atomic Scale Patterning of Freestanding Monolayer Graphene at Elevated Temperature. *ACS Nano* **2013**, *7*, 1566–1572.
37. Han, X.; Funk, M. R.; Shen, F.; Chen, Y.-C.; Li, Y.; Campbell, C. J.; Dai, J.; Yang, X.; Kim, J.-W.; Liao, Y. Scalable Holey Graphene Synthesis and Dense Electrode Fabrication toward High-Performance Ultracapacitors. *ACS Nano* **2014**, *8*, 8255–8265.
38. Nam, S.; Choi, I.; Fu, C.-c.; Kim, K.; Hong, S.; Choi, Y.; Zettl, A.; Lee, L. P. Graphene Nanopore with a Self-Integrated Optical Antenna. *Nano Lett.* **2014**, *14*, 5584–5589.
39. Kuan, A. T.; Lu, B.; Xie, P.; Szalay, T.; Golovchenko, J. A. Electrical Pulse Fabrication of Graphene Nanopores in Electrolyte Solution. *Appl. Phys. Lett.* **2015**, *106*, 203109.
40. Han, P.; Mantooth, B. A.; Sykes, E. C. H.; Donhauser, Z. J.; Weiss, P. S. Benzene on Au{111} at 4 K: Monolayer Growth and Tip-Induced Molecular Cascades. *J. Am. Chem. Soc.* **2004**, *126*, 10787–10793.
41. Sykes, E. C. H.; Mantooth, B. A.; Han, P.; Donhauser, Z. J.; Weiss, P. S. Substrate-Mediated Intermolecular Interactions: A Quantitative Single Molecule Analysis. *J. Am. Chem. Soc.* **2005**, *127*, 7255–7260.
42. Mantooth, B. A.; Sykes, E. C. H.; Han, P.; Moore, A. M.; Donhauser, Z. J.; Crespi, V. H.; Weiss, P. S. Analyzing the Motion of Benzene on Au{111}: Single Molecule Statistics from Scanning Probe Images. *J. Phys. Chem. C* **2007**, *111*, 6167–6182.
43. Heimel, G.; Duhm, S.; Salzmann, I.; Gerlach, A.; Strozecka, A.; Niederhausen, J.; Bürker, C.; Hosokai, T.; Fernandez-Torrente, I.; Schulze, G.; *et al.* Charged and metallic molecular monolayers through surface-induced aromatic stabilization. *Nat. Chem.* **2013**, *5*, 187–194.
44. Ishigami, M.; Chen, J. H.; Cullen, W. G.; Fuhrer, M. S.; Williams, E. D. Atomic Structure of Graphene on SiO_2. *Nano Lett.* **2007**, *7*, 1643–1648.
45. Liao, L.; Bai, J.; Cheng, R.; Lin, Y.-C.; Jiang, S.; Huang, Y.; Duan, X. Top-Gated Graphene Nanoribbon Transistors with Ultrathin High-k Dielectrics. *Nano Lett.* **2010**, *10*, 1917–1921.
46. Liao, L.; Bai, J.; Qu, Y.; Huang, Y.; Duan, X. Single-Layer Graphene on Al_2O_3/Si Substrate: Better Contrast and Higher Performance of Graphene Transistors. *Nanotechnology* **2010**, *21*, 015705.
47. Liang, X.; Sperling, B. A.; Calizo, I.; Cheng, G.; Hacker, C. A.; Zhang, Q.; Obeng, Y.; Yan, K.; Peng, H.; Li, Q. Toward Clean and Crackless Transfer of Graphene. *ACS Nano* **2011**, *5*, 9144–9153.
48. Monnell, J. D.; Stapleton, J. J.; Dirk, S. M.; Reinerth, W. A.; Tour, J. M.; Allara, D. L.; Weiss, P. S. Relative Conductances of Alkaneselenolate and Alkanethiolate Monolayers on Au{111}. *J. Phys. Chem. B* **2005**, *109*, 20343–20349.
49. Han, P.; Kurland, A. R.; Giordano, A. N.; Nanayakkara, S. U.; Blake, M. M.; Pochas, C. M.; Weiss, P. S. Heads and Tails: Simultaneous Exposed and Buried Interface Imaging of Monolayers. *ACS Nano* **2009**, *3*, 3115–3121.

50. Claridge, S. A.; Schwartz, J. J.; Weiss, P. S. Electrons, Photons, and Force: Quantitative Single-Molecule Measurements from Physics to Biology. *ACS Nano* **2011**, *5*, 693–729.
51. Bumm, L. A.; Arnold, J. J.; Charles, L. F.; Dunbar, T. D.; Allara, D. L.; Weiss, P. S. Directed Self-Assembly to Create Molecular Terraces with Molecularly Sharp Boundaries in Organic Monolayers. *J. Am. Chem. Soc.* **1999**, *121*, 8017–8021.
52. Khomyakov, P. A.; Giovannetti, G.; Rusu, P. C.; Brocks, G.; van den Brink, J.; Kelly, P. J. First-Principles Study of the Interaction and Charge Transfer between Graphene and Metals. *Phys. Rev. B: Condens. Matter Mater. Phys.* **2009**, *79*, 195425.
53. Wofford, J. M.; Starodub, E.; Walter, A. L.; Nie, S.; Bostwick, A.; Bartelt, N. C.; Thürmer, K.; Rotenberg, E.; McCarty, K. F.; Dubon, O. D. Extraordinary Epitaxial Alignment of Graphene Islands on Au(111). *New J. Phys.* **2012**, *14*, 053008.
54. Donhauser, Z. J.; Price, D. W.; Tour, J. M.; Weiss, P. S. Control of Alkanethiolate Monolayer Structure Using Vapor-Phase Annealing. *J. Am. Chem. Soc.* **2003**, *125*, 11462–11463.
55. Dameron, A. A.; Charles, L. F.; Weiss, P. S. Structures and Displacement of 1-Adamantanethiol Self-Assembled Monolayers on Au{111}. *J. Am. Chem. Soc.* **2005**, *127*, 8697–8704.
56. Mullen, T. J.; Dameron, A. A.; Saavedra, H. M.; Williams, M. E.; Weiss, P. S. Dynamics of Solution Displacement in 1-Adamantanethiolate Self-Assembled Monolayers. *J. Phys. Chem. C* **2007**, *111*, 6740–6746.
57. Dameron, A. A.; Mullen, T. J.; Hengstebeck, R. W.; Saavedra, H. M.; Weiss, P. S. Origins of Displacement in 1-Adamantanethiolate Self-Assembled Monolayers. *J. Phys. Chem. C* **2007**, *111*, 6747–6752.
58. Saavedra, H. M.; Barbu, C. M.; Dameron, A. A.; Mullen, T. J.; Crespi, V. H.; Weiss, P. S. 1-Adamantanethiolate Monolayer Displacement Kinetics Follow a Universal Form. *J. Am. Chem. Soc.* **2007**, *129*, 10741–10746.
59. Fujii, S.; Akiba, U.; Fujihira, M. Geometry for Self-Assembling of Spherical Hydrocarbon Cages with Methane Thiolates on Au(111). *J. Am. Chem. Soc.* **2002**, *124*, 13629–13635.
60. Kondoh, H.; Kodama, C.; Nozoye, H. Structure-Dependent Change of Desorption Species from *n*-Alkanethiol Monolayers Adsorbed on Au(111): Desorption of Thiolate Radicals from Low-Density Structures. *J. Phys. Chem. B* **1998**, *102*, 2310–2312.
61. Kondoh, H.; Kodama, C.; Sumida, H.; Nozoye, H. Molecular Processes of Adsorption and Desorption of Alkanethiol Monolayers on Au(111). *J. Chem. Phys.* **1999**, *111*, 1175–1184.
62. Gao, L.; Ren, W.; Xu, H.; Jin, L.; Wang, Z.; Ma, T.; Ma, L.-P.; Zhang, Z.; Fu, Q.; Peng, L.-M. Repeated Growth and Bubbling Transfer of Graphene with Millimetre-Size Single-Crystal Grains Using Platinum. *Nat. Commun.* **2012**, *3*, 699.
63. Suk, J. W.; Kitt, A.; Magnuson, C. W.; Hao, Y.; Ahmed, S.; An, J.; Swan, A. K.; Goldberg, B. B.; Ruoff, R. S. Transfer of CVD-Grown Monolayer Graphene onto Arbitrary Substrates. *ACS Nano* **2011**, *5*, 6916–6924.
64. Kang, J.; Hwang, S.; Kim, J. H.; Kim, M. H.; Ryu, J.; Seo, S. J.; Hong, B. H.; Kim, M. K.; Choi, J.-B. Efficient Transfer of Large-Area Graphene Films onto Rigid Substrates by Hot Pressing. *ACS Nano* **2012**, *6*, 5360–5365.
65. Chen, X.-D.; Liu, Z.-B.; Zheng, C.-Y.; Xing, F.; Yan, X.-Q.; Chen, Y.; Tian, J.-G. High-Quality and Efficient Transfer of Large-Area Graphene Films onto Different Substrates. *Carbon* **2013**, *56*, 271–278.
66. Müllen, K. Evolution of Graphene Molecules: Structural and Functional Complexity as Driving Forces behind Nanoscience. *ACS Nano* **2014**, *8*, 6531–6541.
67. Han, P.; Akagi, K.; Canova, F. F.; Mutoh, H.; Shiraki, S.; Iwaya, K.; Weiss, P. S.; Asao, N.; Hitosugi, T. Bottom-Up Graphene-Nanoribbon Fabrication Reveals Chiral Edges and Enantioselectivity. *ACS Nano* **2014**, *8*, 9181–9187.
68. Narita, A.; Verzhbitskiy, I. A.; Frederickx, W.; Mali, K. S.; Jensen, S. A.; Hansen, M. R.; Bonn, M.; De Feyter, S.; Casiraghi, C.; Feng, X. Bottom-Up Synthesis of Liquid-Phase-Processable Graphene Nanoribbons with Near-Infrared Absorption. *ACS Nano* **2014**, *8*, 11622–11630.
69. Zhang, R.; Lyu, G.; Chen, C.; Lin, T.; Liu, J.; Liu, P. N.; Lin, N. Two-Dimensional Superlattices of Bi Nanoclusters Formed on a Au(111) Surface Using Porous Supramolecular Templates. *ACS Nano* **2015**, *9*, 8547–8553.
70. Leong, W. S.; Nai, C. T.; Thong, J. T. L. What Does Annealing Do to Metal–Graphene Contacts? *Nano Lett.* **2014**, *14*, 3840–3847.
71. Hohman, J. N.; Zhang, P.; Morin, E. I.; Han, P.; Kim, M.; Kurland, A. R.; McClanahan, P. D.; Balema, V. P.; Weiss, P. S. Self-Assembly of Carboranethiol Isomers on Au{111}: Intermolecular Interactions Determined by Molecular Dipole Orientations. *ACS Nano* **2009**, *3*, 527–536.